Preconditioners for PDE-constrained optimization problems with box constraints: Towards high resolution inverse ECG images

Ole Løseth Elvetun*and Bjørn Fredrik Nielsen†

June 24, 2015

Abstract

By combining the Minimal Residual Method and the Primal-Dual Active Set algorithm, we derive an efficient scheme for solving a class of PDE-constrained optimization problems with inequality constraints. The approach studied in this paper addresses box constrains on the control function, and leads to an iterative scheme in which linear optimality systems must be solved in each iteration. We prove that the spectra of the associate saddle point operators, appearing in each iteration, are well behaved: Almost all the eigenvalues are contained in three bounded intervals, not containing zero. In fact, for severely ill-posed problems, the number of eigenvalues outside these three intervals are of order $O(\ln(\alpha^{-1}))$ as $\alpha \to 0$, where α is the parameter employed in the Tikhonov regularization. Krylov subspace methods are well known to handle such systems of algebraic equations very well, and we thus obtain a fast method for PDE-constrained optimization problems with box constraints. In contrast to previous papers, our investigation is not targeted at analyzing a specific model, but instead covers a rather large class of problems.

Our theoretical findings are illuminated by several numerical experiments. An example covered by our theoretical findings, as well as cases not fulfilling all the assumptions needed in the analysis, are presented. Also, in addition to computations only involving synthetic data, we briefly explore whether these new techniques can be applied to real world problems. More specifically, the algorithm is tested on a medical imaging problem with clinical patient data. These tests suggest that the method is fast and reliable.

*Department of Mathematical Sciences and Technology, Norwegian University of Life Sciences, Norway. Email: ole.elvetun@nmbu.no

†Department of Mathematical Sciences and Technology, Norwegian University of Life Sciences, Norway; Simula Research Laboratory; Center for Cardiological Innovation, Oslo University Hospital. Email: bjorn.f.nielsen@nmbu.no

Keywords: PDE-constrained optimization, Primal-Dual Active Set, Minimal Residual Method, Real World Applications.

AMS subject classifications: 65F22, 49J20, 35Q93, 65K10

1 Introduction

In the field of optimization many researchers have studied the minimization of quadratic cost-functionals with constraints given by partial differential equations. Several books have been written about this subject, see e.g [3, 5, 7, 15]. By using the Lagrange multiplier technique, one might derive a system of equations which must be satisfied by the optimal solution. After suitable discretization, this system, which typically is a saddle-point problem, can be solved by an all-at-once method. That is, a scheme in which the primal, dual and optimality conditions are solved in a fully coupled manner.

Such optimality systems are often ill-posed, which leads to bad condition numbers for the discretized systems, and regularization techniques must therefore be invoked. Typically, if Tikhonov regularization is employed, then the spectral condition number of the system is of order $O(\alpha^{-1})$, where $\alpha > 0$ is the regularization parameter. Hence one might expect that, for small values of α, the number of iterations required to solve the system, using e.g. Krylov subspace methods, would be large. However, in [11] the authors prove that the spectrum of the optimality system consists of three bounded intervals and a very limited number of isolated eigenvalues outside these three intervals. This result is established for a quite broad class of PDE constrained optimization problems and imply that the Minimal Residual Method (MINRES) will handle the associated algebraic systems very well. In fact, if the problem at hand is severely ill-posed, then the required number of iterations cannot grow faster than $O([\ln(\alpha^{-1})]^2)$ as $\alpha \to 0$, and in practice one often observes iterations counts of order $O(\ln(\alpha^{-1}))$.

Many real world problems are not only modeled by PDEs, but also involve inequality constraints. These are often given in the form of box constraints on the control function. In this paper we explore whether the method and analysis presented in [11] can be extended to handle such problems adequately.

Inequality constraints typically require the use of an iterative method to solve the overall optimization task. In consequence, since the linear systems arising in each iteration typically are ill-posed, we need to solve a sequence of algebraic systems with bad condition numbers.

For some specific state equations, such problems have been solved efficiently, see e.g. [4, 14]. These efficient techniques also combines the cherished PDAS method in [2] with different numerical techniques for solving saddle-point problems [1]. We will consider such optimization tasks in a

more abstract and general setting. More precisely, our analysis concerns the class of problems that can be written on the form

$$\min_{(v,u)\in L^2(\Omega_v)\times U} \left\{ \frac{1}{2}\|Tu-d\|_Z^2 + \frac{1}{2}\alpha\|v\|_{L^2(\Omega_v)}^2 \right\}, \tag{1}$$

subject to

$$Au + Bv = 0, \tag{2}$$
$$v(x) \geq 0 \text{ a.e. in } \Omega_v, \tag{3}$$

where

- $L^2(\Omega_v)$ is the control space,
- U is the state space, $1 \leq \dim(U) \leq \infty$, and
- Z is the observation space, $1 \leq \dim(Z) \leq \infty$.

We assume that U and Z are Hilbert spaces. Further, $\Omega_v \subset \mathbb{R}^n$ is the domain the control function v is defined on, d is the given observation data, and $\alpha > 0$ is the regularization parameter. In Section 2 we will state the assumptions we need on the linear operators A, B and T. Also, there exists a solution to the problem (1)-(3) under fairly loose assumptions. For $\alpha > 0$, the solution is unique, see e.g. [5] for details.

For the problem (1)-(2), without the inequality constraint $v(x) \geq 0$, it was proven in [11] that for a sound discretization of the associated KKT system

$$\underbrace{\begin{bmatrix} \alpha I & 0 & B^* \\ 0 & T^*T & A^* \\ B & A & 0 \end{bmatrix}}_{=\mathcal{B}_\alpha} \begin{bmatrix} v \\ u \\ w \end{bmatrix} = \begin{bmatrix} 0 \\ T^*d \\ 0 \end{bmatrix}, \tag{4}$$

the eigenvalues of the discretized operator $\mathcal{B}_\alpha^h$ satisfies

$$\text{sp}(\mathcal{B}_\alpha^h) \subset [-b,-a] \cup [c\alpha, 2\alpha] \cup \{\lambda_1, \lambda_2, ..., \lambda_{N(\alpha)}\} \cup [a,b]. \tag{5}$$

Here, a, b and c are constants, independent of the regularization parameter α, and $N(\alpha) = O(\ln(\alpha^{-1}))$ for severely ill-posed problems. Krylov subspace methods handle problems with spectra on the form (5) very well, and, since we have an indefinite system, the Minimal Residual (MINRES) method [12] is well suited for solving (4).

Based on this discussion, we can formulate the objectives of this paper as follows:

- We will combine the PDAS method, presented in [2], with the MINRES method used in [11] to obtain a standard recipe for solving problems

of the form (1)-(3). We prove that in each iteration of the PDAS algorithm we obtain a reduced system with a spectrum on the form (5), which we then can solve efficiently with the MINRES algorithm. Our derivation of the reduced systems, arising in the PDAS method, is heavily inspired by [4, 14]. Moreover, in the numerical experiments section, we show how to apply Riesz maps as preconditioners to solve some model problems.

- Real world problems often involve highly unstructured meshes and noisy data. Our second objective is to undertake a numerical investigation of such a real world PDE-constrained optimization problem, known as *the inverse problem of electrocardiography (ECG)*. The aim is to identify a heart infarct using ECG recordings and PDE-constrained optimization with box constraints. This problem has an H^1-control function, and is therefore not supported by the analysis of (1)-(3). Nevertheless, our scheme converged, and seemed to improve the quality of the solution - compared to the solution without box constraints.

For practical PDE-constrained optimization problems, the condition numbers of the discretized KKT systems is known to increase significantly, not only as the regularization parameter $\alpha \to 0$, but also when the mesh parameter $h > 0$ decreases. We will not discuss this generally, but for the synthetic model problem, we will explain how to handle the h-dependency by invoking Riesz maps as multigrid preconditioners. We then obtain an algorithm robust with respect to h and which grows moderately in iteration numbers as $\alpha \to 0$.

Remark 1.1. *We consider the prototypical inequality constraint $v(x) \geq 0$, since the aim of this paper is to show that the linear systems occurring in each iteration of the PDAS algorithm can be efficiently solved with the MINRES method, and the simple constraint $v(x) \geq 0$ makes the derivation and analysis more transparent. To see how to handle the more general box constraints*

$$v_l(x) \leq v(x) \leq v_u(x),$$

see e.g. [16, 14]. Also note that the requirement $v(x) \geq 0$ occurs in many applications, e.g., when the control function v measures density, temperature, mass or pressure.

2 Assumptions

We assume that:

$\mathcal{A}\mathbf{1}$: $A : U \to U$ is bounded and linear[1]

[1]Assume that the state equation (2) is a PDE. Then, A is typically a mapping from

$\mathcal{A}\mathbf{2}$: A^{-1} exists and is bounded.

$\mathcal{A}\mathbf{3}$: $B : L^2(\Omega_v) \to U$ is bounded and linear.

$\mathcal{A}\mathbf{4}$: $T : U \to Z$ is bounded and linear.

$\mathcal{A}\mathbf{5}$: The optimization problem (1)-(2) is severely ill-posed for $\alpha = 0$.

As shown in [11], if the assumptions listed above hold, then for a sound discretization of the KKT system (4), the eigenvalues of this discretized system satisfies (5). If (4) is well posed for $\alpha = 0$, then the numerical solution of this problem is "straightforward" and regularization is not needed. We will focus on the challenging case, i.e. severely ill-posed systems.

3 KKT system

We will now derive the algorithm for solving (1)-(3). The first thing we need, is the optimality system, which can be obtained from the Lagrangian

$$\mathcal{L}(v, u, w, \lambda) = \frac{1}{2}\|Tu - d\|_Z^2 + \frac{1}{2}\alpha\|v\|_{L^2(\Omega_v)}^2 + (w, Au + Bv)_U - (\lambda, v)_{L^2(\Omega_v)}. \quad (6)$$

The standard optimality theory states that if (v^*, u^*) is a solution of (1)-(3), then there exist duality functions (w^*, λ^*) such that the Fréchet derivatives of (6), with respect to v, u and w,

$$\left\langle \frac{\partial \mathcal{L}}{\partial v}, \phi \right\rangle = (\alpha v, \phi)_{L^2(\Omega_v)} + (B\phi, w)_U - (\lambda, \phi)_{L^2(\Omega_v)}, \ \forall \phi \in L^2(\Omega_v),$$
$$\left\langle \frac{\partial \mathcal{L}}{\partial u}, \phi \right\rangle = (Tu - d, T\phi)_Z + (A\phi, w)_U, \ \forall \phi \in U,$$
$$\left\langle \frac{\partial \mathcal{L}}{\partial w}, \phi \right\rangle = (Au + Bv, \phi)_U, \ \forall \phi \in U,$$

should all be equal to zero at the optimal point $(v^*, u^*, w^*, \lambda^*)$. In addition, the conditions given by

$$(\lambda v)(x) = 0, \quad (7)$$
$$\lambda(x), v(x) \geq 0, \quad (8)$$

should also be satisfied at this optimal point. By writing the Fréchet derivatives on block form, we get the well known KKT system

$$\begin{bmatrix} \alpha I & 0 & B^* \\ 0 & T^*T & A^* \\ B & A & 0 \end{bmatrix} \begin{bmatrix} v \\ u \\ w \end{bmatrix} = \begin{bmatrix} \lambda \\ T^*d \\ 0 \end{bmatrix}, \quad (9)$$

U onto its dual space U', and hence $\mathcal{A}\mathbf{1}$ is not fulfilled. This can, nevertheless, easily be rectified by applying the inverse Riesz map $R_U^{-1} : U' \to U$ to (2) and thereby obtain the operator $R_U^{-1}A : U \to U$. In this context, one might consider R_U^{-1} to be a preconditioner. We will return to this issue in the example sections.

which we combine with (7)-(8) to obtain the full optimality system. Note that, since we have a convex problem, a solution $(v^*, u^*, w^*, \lambda^*)$ of (7)-(9) will also be a solution of (1)-(3).

4 Primal-dual active set method

To solve our optimization problem, we will follow the primal-dual technique introduced in [2], and later used in [4] and [14].

Thus, we start by noting that (7)-(8) are equivalent to the condition

$$\lambda + \min(0, cv - \lambda) = 0 \quad \forall c > 0.$$

This motivates the PDAS algorithm, where we can define the active $\mathcal{A}$ and inactive $\mathcal{I}$ sets as follows

$$\mathcal{A} = \{x \in \Omega_v : (cv - \lambda)(x) < 0\}, \tag{10}$$

$$\mathcal{I} = \Omega_v \setminus \mathcal{A}, \tag{11}$$

where Ω_v is the domain of the control v. We can now formulate the PDAS method for solving our optimality problem (1)-(3). In the iterative procedure, we need to solve systems on the form (9) at each step, i.e., solve

$$\begin{bmatrix} \alpha I & 0 & B^* \\ 0 & T^*T & A^* \\ B & A & 0 \end{bmatrix} \begin{bmatrix} v^k \\ u^k \\ w^k \end{bmatrix} = \begin{bmatrix} \lambda^k \\ T^*d \\ 0 \end{bmatrix}, \tag{12}$$

together with

$$\lambda^k(x) = 0 \quad \text{on } \mathcal{I}^k, \tag{13}$$

$$v^k(x) = 0 \quad \text{on } \mathcal{A}^k. \tag{14}$$

Note that the unknowns are v^k, u^k, w^k and λ^k, and hence there are unknowns on both sides of equation (12). Here, $\mathcal{A}^k$ and $\mathcal{I}^k$ are the active and inactive sets associated with the kth iteration of the PDAS algorithm, see steps 9 and 10 in Algorithm 1.

In [2] it is shown that the primal-dual active set method provides a local minimum if the active set stays unchanged in two consecutive iterations. We can now, schematically, present the PDAS algorithm, see Algorithm 1.

Although the algorithm is in place, it is possible to reduce the CPU cost of solving (12) - (14). The idea is based on the fact that, at each iteration, we know that the control parameter v^k is zero on the active domain (14), and similarly, we know that the Lagrange multiplier λ^k is zero on the inactive domain (13). Hence, it intuitively seems possible to restrict the control v^k to the inactive domain. Similarly, we want to restrict the Lagrange multiplier λ^k to the active domain. By restricting these functions, the optimality system to be solved becomes smaller, in the sense of fewer indices in the corresponding discretized KKT equations, and hence it will be faster to solve.

Algorithm 1 Primal-dual active-set method

Choose the initial set $\mathcal{A}^0$ of active constraints
$\mathcal{I}^0 = \Omega_v \setminus \mathcal{A}^0$
for k = 0, 1, 2,... **do**
  if $k > 0$ and $\mathcal{A}^k = \mathcal{A}^{k-1}$ **then**
    STOP (algorithm converged)
  else
    Solve (12) - (14)
  end if
  $\mathcal{A}^{k+1} = \{x \in \Omega_v : (cv^k - \lambda^k)(x) < 0\}$
  $\mathcal{I}^{k+1} = \Omega_v \setminus \mathcal{A}^{k+1}$
end for

5 Reduced KKT system

We will now first derive a linear system which only involves the restrictions of v^k and λ^k to the inactive and active domains, respectively. Thereafter, we analyze whether assumptions $\mathcal{A}\mathbf{1}$-$\mathcal{A}\mathbf{5}$, see Section 2, are inherited by this system.

Let $q \in L^2(\Omega_v)$ be arbitrary. We may split $q \in L^2(\Omega_v)$,

$$q(x) = \begin{cases} q^{\mathcal{I}^k}(x) & \text{if } x \in \mathcal{I}^k, \\ q^{\mathcal{A}^k}(x) & \text{if } x \in \mathcal{A}^k. \end{cases} \tag{15}$$

where

$$q^{\mathcal{I}^k} = q|_{\mathcal{I}^k},$$
$$q^{\mathcal{A}^k} = q|_{\mathcal{A}^k}.$$

Let us also introduce the notation

$$L^2(\mathcal{I}^k) = \{q|_{\mathcal{I}^k} : q \in L^2(\Omega_v)\}, \tag{16}$$
$$L^2(\mathcal{A}^k) = \{q|_{\mathcal{A}^k} : q \in L^2(\Omega_v)\},$$

and note that

$$q^{\mathcal{I}^k} \in L^2(\mathcal{I}^k),$$
$$q^{\mathcal{A}^k} \in L^2(\mathcal{A}^k).$$

To derive the reduced KKT system, we need an operator which maps the restricted function $v^{\mathcal{I}^k}$ of the control v^k into the entire control space $L^2(\Omega_v)$. This operator must map a function defined on the domain $\mathcal{I}^k$ into a function defined on the domain Ω_v by employing a zero extension. We will denote this operator by

$$E^{\mathcal{I}^k} : L^2(\mathcal{I}^k) \to L^2(\Omega_v). \tag{17}$$

Note that, for any $r \in L^2(\mathcal{I}^k)$,

$$\left(E^{\mathcal{I}^k} r\right)(x) = r(x) \quad \text{for all } x \in \mathcal{I}^k, \tag{18}$$

$$\left(E^{\mathcal{I}^k} r\right)(x) = 0 \quad \text{for all } x \in \mathcal{A}^k. \tag{19}$$

We also need a similar operator $E^{\mathcal{A}^k}$ for the Lagrange multiplier λ^k. That is, an operator which maps the restricted version $\lambda^{\mathcal{A}^k}$ of λ^k into the full domain Ω_v, by a zero extension. Formally, this is defined as

$$E^{\mathcal{A}^k} : L^2(\mathcal{A}^k) \to L^2(\Omega_v),$$

where this mapping satisfies

$$\left(E^{\mathcal{A}^k} r\right)(x) = r(x) \quad \text{for all } x \in \mathcal{A}^k, \tag{20}$$

$$\left(E^{\mathcal{A}^k} r\right)(x) = 0 \quad \text{for all } x \in \mathcal{I}^k, \tag{21}$$

which holds for any $r \in L^2(\mathcal{A}^k)$. From (18)-(19) and (20)-(21), we can define the inner products of the "restricted" spaces $L^2(\mathcal{I}^k)$ and $L^2(\mathcal{A}^k)$ as

$$(q, r)_{L^2(\mathcal{I}^k)} = (E^{\mathcal{I}^k} q, E^{\mathcal{I}^k} r)_{L^2(\Omega_v)}, \tag{22}$$

$$(q, r)_{L^2(\mathcal{A}^k)} = (E^{\mathcal{A}^k} q, E^{\mathcal{A}^k} r)_{L^2(\Omega_v)}. \tag{23}$$

By construction, $\mathcal{I}^k \cap \mathcal{A}^k = \emptyset$, and (19) and (21) therefore imply that the ranges of $E^{\mathcal{I}^k}$ and $E^{\mathcal{A}^k}$ are orthogonal sets in $L^2(\Omega_v)$,

$$R\left(E^{\mathcal{I}^k}\right) \perp R\left(E^{\mathcal{A}^k}\right). \tag{24}$$

Also note that $E^{\mathcal{I}^k}$ and $E^{\mathcal{A}^k}$ are one-to-one, but not onto. Due to (18)-(19) and (20)-(21), all $q \in L^2(\Omega_v)$ satisfy

$$q = E^{\mathcal{I}^k} q^{\mathcal{I}^k} + E^{\mathcal{A}^k} q^{\mathcal{A}^k}, \tag{25}$$

cf. the splitting (15).

Recall that the linear operator B maps the control in $L^2(\Omega_v)$ into the state space U, see sections 1 and 2. We can now use (25) to conveniently split this mapping:

$$\begin{aligned} Bq &= BE^{\mathcal{I}^k} q^{\mathcal{I}^k} + BE^{\mathcal{A}^k} q^{\mathcal{A}^k} \\ &= B^{\mathcal{I}^k} q^{\mathcal{I}^k} + B^{\mathcal{A}^k} q^{\mathcal{A}^k}, \end{aligned} \tag{26}$$

where

$$B^{\mathcal{I}^k} = BE^{\mathcal{I}^k} : L^2(\mathcal{I}^k) \to U, \tag{27}$$

$$B^{\mathcal{A}^k} = BE^{\mathcal{A}^k} : L^2(\mathcal{A}^k) \to U, \tag{28}$$

With these operators at hand, we are now able to simplify the optimality system (12) - (14). We start with formulating the following lemma.

Lemma 5.1. *Let $E^{\mathcal{I}^k}$ and $E^{\mathcal{A}^k}$ be the extension operators introduced in (18)-(19) and (20)-(21), respectively. Then*

(i) $q = E^{\mathcal{I}^k} q^{\mathcal{I}^k} + E^{\mathcal{A}^k} q^{\mathcal{A}^k}$ *for any* $q \in L^2(\Omega_v)$,

(ii) $Bq = B^{\mathcal{I}^k} q^{\mathcal{I}^k} + B^{\mathcal{A}^k} q^{\mathcal{A}^k}$ *for any* $q \in L^2(\Omega_v)$,

(iii) $B^* = E^{\mathcal{I}^k}[B^{\mathcal{I}^k}]^* + E^{\mathcal{A}^k}[B^{\mathcal{A}^k}]^*$,

where $B^{\mathcal{I}^k}$ and $B^{\mathcal{A}^k}$ are defined in (27) and (28), respectively.

Proof. (i) was established in the derivation leading to (25).

(ii) was established in the derivation leading to (26).

(iii) can be verified has follows. First, (18)-(19) and (20)-(21) imply that, for any $q, r \in L^2(\Omega_v)$,

$$\begin{aligned} (q^{\mathcal{I}^k}, r^{\mathcal{I}^k})_{L^2(\mathcal{I}^k)} &= (q, E^{\mathcal{I}^k} r^{\mathcal{I}^k})_{L^2(\Omega_v)}, \\ (q^{\mathcal{A}^k}, r^{\mathcal{A}^k})_{L^2(\mathcal{A}^k)} &= (q, E^{\mathcal{A}^k} r^{\mathcal{A}^k})_{L^2(\Omega_v)}. \end{aligned}$$

Consequently, for arbitrary $q \in L^2(\Omega_v)$ and $s \in U$,

$$\begin{aligned} (q, B^* s)_{L^2(\Omega_v)} &= (Bq, s)_U \\ &= (B^{\mathcal{I}^k} q^{\mathcal{I}^k} + B^{\mathcal{A}^k} q^{\mathcal{A}^k}, s)_U \\ &= \left(q^{\mathcal{I}^k}, [B^{\mathcal{I}^k}]^* s\right)_{L^2(\mathcal{I}^k)} + \left(q^{\mathcal{A}^k}, [B^{\mathcal{A}^k}]^* s\right)_{L^2(\mathcal{A}^k)} \\ &= \left(q, E^{\mathcal{I}^k}[B^{\mathcal{I}^k}]^* s\right)_{L^2(\Omega_v)} + \left(q, E^{\mathcal{A}^k}[B^{\mathcal{A}^k}]^* s\right)_{L^2(\Omega_v)} \\ &= \left(q, \left\{E^{\mathcal{I}^k}[B^{\mathcal{I}^k}]^* + E^{\mathcal{A}^k}[B^{\mathcal{A}^k}]^*\right\} s\right)_{L^2(\Omega_v)}. \end{aligned}$$

Hence, it follows that $B^* = E^{\mathcal{I}^k}[B^{\mathcal{I}^k}]^* + E^{\mathcal{A}^k}[B^{\mathcal{A}^k}]^*$, which finishes the proof.

□

Assume that v^k, u^k, w^k and λ^k satisfy (12)-(14), i.e.

$$\alpha v^k + B^* w^k = \lambda^k, \tag{29}$$

$$T^* T u^k + A^* w^k = T^* d, \tag{30}$$

$$B v^k + A u^k = 0, \tag{31}$$

$$\lambda^k = 0 \text{ on } \mathcal{I}^k, \tag{32}$$

$$v^k = 0 \text{ on } \mathcal{A}^k. \tag{33}$$

From properties (i) and (iii) in Lemma 5.1 we find that equation (29) may be written on the form

$$\begin{aligned}\alpha v^k + B^* w^k &= \alpha E^{\mathcal{I}^k} v^{\mathcal{I}^k} + \alpha E^{\mathcal{A}^k} v^{\mathcal{A}^k} + E^{\mathcal{I}^k} [B^{\mathcal{I}^k}]^* w^k + E^{\mathcal{A}^k} [B^{\mathcal{A}^k}]^* w^k \\ &= E^{\mathcal{I}^k} \lambda^{\mathcal{I}^k} + E^{\mathcal{A}^k} \lambda^{\mathcal{A}^k} = \lambda^k.\end{aligned}$$

Since $\lambda^{\mathcal{I}^k} = 0$ and $v^{\mathcal{A}^k} = 0$,

$$\alpha E^{\mathcal{I}^k} v^{\mathcal{I}^k} + E^{\mathcal{I}^k} [B^{\mathcal{I}^k}]^* w^k + E^{\mathcal{A}^k} [B^{\mathcal{A}^k}]^* w^k = E^{\mathcal{A}^k} \lambda^{\mathcal{A}^k}$$

or

$$E^{\mathcal{I}^k} \left\{ \alpha v^{\mathcal{I}^k} + [B^{\mathcal{I}^k}]^* w^k \right\} + E^{\mathcal{A}^k} \left\{ [B^{\mathcal{A}^k}]^* w^k - \lambda^{\mathcal{A}^k} \right\} = 0. \tag{34}$$

But recall that the ranges of $E^{\mathcal{I}^k}$ and $E^{\mathcal{A}^k}$ are orthogonal, cf. (24), and that these operators are one-to-one. Consequently, we find that (34) can be split into two equations

$$\begin{aligned}\alpha v^{\mathcal{I}^k} + [B^{\mathcal{I}^k}]^* w^k &= 0, \\ [B^{\mathcal{A}^k}]^* w^k - \lambda^{\mathcal{A}^k} &= 0,\end{aligned}$$

which implies that (29) can be replaced with these two expressions.

Next, we can use property (ii) in Lemma 5.1 to express equation (31) as

$$B v^k + A u^k = B^{\mathcal{I}^k} v^{\mathcal{I}^k} + B^{\mathcal{A}^k} v^{\mathcal{A}^k} + A u^k = 0$$

or

$$B^{\mathcal{I}^k} v^{\mathcal{I}^k} + A u^k = 0,$$

where we have used that $v^{\mathcal{A}^k} = 0$.

The KKT system (29)-(33) can therefore be written on the form

$$\begin{aligned}\alpha v^{\mathcal{I}^k} + [B^{\mathcal{I}^k}]^* w^k &= 0, \\ [B^{\mathcal{A}^k}]^* w^k - \lambda^{\mathcal{A}^k} &= 0, \\ T^* T u^k + A^* w^k &= T^* d, \\ B^{\mathcal{I}^k} v^{\mathcal{I}^k} + A u^k &= 0,\end{aligned}$$

Proposition 5.2. *Assume that v^k, u^k, w^k and λ^k solve (12)-(14). Then $v^{\mathcal{I}^k} = v^k|_{\mathcal{I}^k}$, u^k, w^k and $\lambda^{\mathcal{A}^k} = \lambda^k|_{\mathcal{A}^k}$ satisfy*

$$\underbrace{\begin{bmatrix} \alpha I^{\mathcal{I}^k} & 0 & [B^{\mathcal{I}^k}]^* \\ 0 & T^*T & A^* \\ B^{\mathcal{I}^k} & A & 0 \end{bmatrix}}_{=\mathcal{B}_\alpha^k} \begin{bmatrix} v^{\mathcal{I}^k} \\ u^k \\ w^k \end{bmatrix} = \begin{bmatrix} 0 \\ T^* d \\ 0 \end{bmatrix}, \tag{35}$$

$$\lambda^{\mathcal{A}^k} = [B^{\mathcal{A}^k}]^* w^k. \tag{36}$$

With other words, in each iteration of the PDAS method we can solve the block system (35) and thereafter use the straightforward update (36) for the Lagrange multiplier.

6 Spectrum of the reduced KKT system

Assume that assumptions $\mathcal{A}\mathbf{1}$-$\mathcal{A}\mathbf{5}$ hold, see Section 2. In the introduction we mentioned that for a sound discretization of (4), associated with (1)-(2), without the inequality constraint (3), the discrete operator $\mathcal{B}_\alpha^h$ has a spectrum of the form (5). This issue is analyzed in detail in [11]. Krylov subspace solvers therefore handle (4) very well. We have shown in the derivation leading to (35) that we get KKT systems very similar to (4) in each iteration of the PDAS algorithm. One might therefore hope that the MINRES method also is a fast solver for the reduced system (35). This issue can be investigated by exploring whether the operators appearing in $\mathcal{B}_\alpha^k$, defined in (35), also satisfy assumptions $\mathcal{A}\mathbf{1}$-$\mathcal{A}\mathbf{5}$. In short, are these properties, assumed to hold for $\mathcal{B}_\alpha$, inherited by $\mathcal{B}_\alpha^k$? If this is the case, then the spectrum of $\mathcal{B}_\alpha^k$ also will consist of three bounded intervals with a few isolated eigenvalues, i.e. be of the form (5), and Krylov solvers will handle (35) well.

We start by pointing out that (35) is the KKT system associated with the following optimization problem:

$$\min_{(v^{\mathcal{I}^k},u)\in L^2(\mathcal{I}^k)\times U} \left\{ \frac{1}{2}\|Tu-d\|_Z^2 + \frac{1}{2}\alpha\|v^{\mathcal{I}^k}\|_{L^2(\mathcal{I}^k)}^2 \right\}, \tag{37}$$

subject to

$$Au = -B^{\mathcal{I}^k} v^{\mathcal{I}^k} = -BE^{\mathcal{I}^k} v^{\mathcal{I}^k}, \tag{38}$$

where $L^2(\mathcal{I}^k)$, $E^{\mathcal{I}^k}$ and $B^{\mathcal{I}^k}$ are defined in the previous section.

We note that (37)-(38) is on the same form as (1)-(2), except that B in (2) has been replaced with $B^{\mathcal{I}^k} = BE^{\mathcal{I}^k}$. Since the operators A and T are unchanged in the reduced problem (37)-(38), we immediately conclude that (35) fulfills assumptions $\mathcal{A}\mathbf{1}$, $\mathcal{A}\mathbf{2}$, and $\mathcal{A}\mathbf{4}$. It remains to explore $\mathcal{A}\mathbf{3}$ and $\mathcal{A}\mathbf{5}$.

Note that assumption $\mathcal{A}\mathbf{3}$ no longer concerns the operator B, but instead the operator

$$B^{\mathcal{I}^k} = BE^{\mathcal{I}^k} : L^2(\mathcal{I}^k) \to U,$$

cf. the derivation leading to (27). Thus, we must prove that

$$E^{\mathcal{I}^k} : L^2(\mathcal{I}^k) \to L^2(\Omega_v),$$

see (17)-(19), is a bounded and linear operator. It is obvious that such an extension operator is linear, and from (18)-(19) and (22) we find that

$$\|E^{\mathcal{I}^k} r\|_{L^2(\Omega_v)} = \|r\|_{L^2(\mathcal{I}^k)} \quad \text{for any } r \in L^2(\mathcal{I}^k),$$

and therefore

$$\|E^{\mathcal{I}^k}\| = \sup_{r\in L^2(\mathcal{I}^k)} \frac{\|E^{\mathcal{I}^k} r\|_{L^2(\Omega_v)}}{\|r\|_{L^2(\mathcal{I}^k)}} = 1. \tag{39}$$

Since B is assumed to be bounded and linear, we can conclude that $B^{\mathcal{I}^k}$ is linear and bounded, i.e. (35) satisfies assumption $\mathcal{A}\mathbf{3}$.

Although we assumed that (1)-(3) is ill-posed without regularization $\alpha = 0$, see assumption $\mathcal{A}\mathbf{5}$ in Section 2, this may not be the case for (37)-(38) (with $\alpha = 0$). For example, if the inactive set $\mathcal{I}^k$ only contains one element/index, then (37)-(38) typically will be well-posed even with zero regularization. Hence, one can in general not assure that $\mathcal{A}\mathbf{5}$, assumed to be satisfied by $\mathcal{B}_0$, is inherited by $\mathcal{B}_0^k$. There are two possibilities:

- If, luckily, (37)-(38) is well posed for $\alpha = 0$, then regularization is not needed, and the effective numerical solution of this linear system with the MINRES method follows from standard theory.

- If $\mathcal{A}\mathbf{5}$ is inherited by (37)-(38), then $\mathcal{A}\mathbf{1}$-$\mathcal{A}\mathbf{5}$ are satisfied, and a sound discretization $\mathcal{B}_\alpha^{k,h}$ of $\mathcal{B}_\alpha^k$ will have eigenvalues satisfying

$$\text{sp}(\mathcal{B}_\alpha^{k,h}) \subset [-b,-a] \cup [c\alpha, 2\alpha] \cup \{\lambda_1, \lambda_2, ..., \lambda_{N(\alpha)}\} \cup [a,b]. \tag{40}$$

  (Of course, the constants in this expression may differ from those in (5)). From this result, and the Chebyschev polynomial analysis presented in [11], it follows that the number of MINRES iterations needed to solve (35) can not grow faster than of order $O([\ln(\alpha^{-1})]^2)$ as $\alpha \to 0$. Moreover, in practical computations one often observes iterations counts of order $O(\ln(\alpha^{-1}))$. (The latter issue is also discussed from a theoretical point of view in [11]).

Definition 6.1 ("Sound discretization")**.** *A "sound discretization" of $\mathcal{B}_\alpha^k$ means that also the discrete problem should satisfy $\mathcal{A}\mathbf{1} - \mathcal{A}\mathbf{4}$, with operator norms which are bounded independently of the mesh parameter h. In addition, a discrete version of $\mathcal{A}\mathbf{5}$ should hold, i.e. that the eigenvalues of $\mathcal{B}_0^{k,h}$ satisfy*

$$|\lambda_i(\mathcal{B}_0^{k,h})| \leq \tilde{c}e^{-\tilde{C}i}, \quad i = 1, ..., n, \tag{41}$$

where $\tilde{c}, \tilde{C}$ are positive constants.

Remark 6.2. *For finite dimensional problems, there obviously always exist $\tilde{c}$ and $\tilde{C}$ such that* (41) *holds. Our results are therefore only of relevance for problems where*

$$\tilde{c}e^{-\tilde{C}n}$$

is extremely close to zero. That is, much smaller than typical choices of the size of the regularization parameter α. The latter will typically be the case if an ill-posed problem is discretized.

Theorem 6.3. *Let $\mathcal{B}_\alpha^k$ be the operator defined in (35). Assume that assumption $\mathcal{A}\mathbf{5}$ is inherited by* (37)-(38)*. Then, for every $\alpha > 0$ and for a*

sound discretization $\mathcal{B}_\alpha^{k,h}$ *of* $\mathcal{B}_\alpha^k$*, in the sense of Definition 6.1, the spectrum of the associated discretized operator obeys*

$$\mathrm{sp}(\mathcal{B}_\alpha^{k,h}) \subset [-b,-a] \cup [c\alpha, 2\alpha] \cup \{\lambda_1, \lambda_2, ..., \lambda_{N(\alpha)}\} \cup [a,b].$$

Here, a*,* b*, and* c *are positive constants independent of* α *and* $N(\alpha) = O(\ln(\alpha^{-1}))$*.*

Since the operators appearing in $\mathcal{B}_\alpha^k$ fulfill assumptions $\mathcal{A}\mathbf{1}$-$\mathcal{A}\mathbf{5}$, the proof of this theorem is identical to the analysis presented in [11], and therefore omitted.

We conclude, at least theoretically, that the MINRES algorithm is well suited for solving the KKT system (35) appearing in each iteration of the PDAS algorithm applied to the box constrained optimization problem (1)-(3). We will illuminate these findings below with numerical experiments.

7 Example 1

In our first model problem we define

$$\begin{aligned}\Omega &= (0,1) \times (0,1),\\ \Omega_v &= \left(\frac{1}{4}, \frac{3}{4}\right) \times \left(\frac{1}{4}, \frac{3}{4}\right),\end{aligned}$$

and consider the minimization problem

$$\min_{(v,u) \in L^2(\Omega_v) \times H^1(\Omega)} \left\{ \frac{1}{2} \|Tu - d\|^2_{L^2(\partial\Omega)} + \frac{1}{2}\alpha \|v\|^2_{L^2(\Omega_v)} \right\} \tag{42}$$

subject to

$$\begin{aligned} -\Delta u + u &= \begin{cases} -v & \text{if } x \in \Omega_v, \\ 0 & \text{if } x \in \Omega \setminus \Omega_v, \end{cases} && (43)\\ \nabla u \cdot n &= 0 \text{ on } \partial\Omega, && (44)\\ v(x) &\geq 0 \text{ a.e.} && (45) \end{aligned}$$

Here, T denotes the trace operator $T : H^1(\Omega) \to L^2(\partial\Omega)$, which is well known to bounded and linear, i.e. assumption $\mathcal{A}\mathbf{4}$ holds. Note that the state space U and the observation space Z are

$$U = H^1(\Omega), \tag{46}$$

$$Z = L^2(\partial\Omega). \tag{47}$$

We are thus trying to recover the function $v \in L^2(\Omega_v)$ from an observation of u along the boundary $\partial\Omega$ of Ω.

Remark 7.1. *We want to derive the optimality system associated with (42)-(45) and to solve it with Algorithm 1. There are, however, two issues that must be handled before we can employ the theoretical considerations presented above:*

(a) In the generic state equation (2) we assumed that the operator A is a mapping from the state space U onto the state space U, i.e. $A : U \to U$. This differs from standard PDE theory. For example, the weak form of (43) involves an operator $\widehat{A}$ mapping $H^1(\Omega)$ onto its dual space $(H^1(\Omega))'$.

(b) In order to solve the KKT system associated with (42)-(45) numerically, we must discretize the operators by applying, e.g., the Finite Element Method (FEM).

Both of these matters can be handled adequately, and we will discuss each of them in some detail. It is, however, difficult to treat both problems simultaneously. Therefore, we address them separately, starting with (a), which will provide us with a suitable preconditioner for the continuous KKT system. Thereafter, we briefly comment the discretization of the preconditioned optimality system, i.e. issue (b).

7.1 Preconditioner

Let us explore issue (a). As mentioned above, the discussion of this matter will provide us with a suitable preconditioner for the KKT system arising in each iteration of the PDAS algorithm applied to solve (42)-(45).

The variational form of (43)-(44) reads: Find $u \in U = H^1(\Omega)$ such that

$$\int_\Omega \nabla u \cdot \nabla \psi + u\psi \, dx = -\int_{\Omega_v} v\psi \, dx \quad \text{for all } \psi \in U,$$

or

$$\langle \widehat{A}u, \psi \rangle = -\langle \widehat{B}v, \psi \rangle \quad \text{for all } \psi \in U, \tag{48}$$

where

$$\widehat{A} : U \to U', \quad u \to \int_\Omega \nabla u \cdot \nabla \psi + u\psi \, dx, \; \psi \in U,$$
$$\widehat{B} : L^2(\Omega_v) \to U', \quad v \to \int_{\Omega_v} v\psi \, dx, \; \psi \in U.$$

We may write (48) more compactly, i.e.

$$\widehat{A}u = -\widehat{B}v.$$

In order to obtain an equation of the form (2), where $A : U \to U$ and $B : L^2(\Omega_v) \to U$, we can simply invoke the inverse R_U^{-1} of the Riesz map $R_U : U \to U'$, i.e.

$$R_U^{-1}\widehat{A}u = -R_U^{-1}\widehat{B}v,$$

which is on the desired form since

$$A = R_U^{-1}\widehat{A} : U \to U, \tag{49}$$

$$B = R_U^{-1}\widehat{B} : L^2(\Omega_v) \to U. \tag{50}$$

From standard theory for elliptic PDEs, it follows that A, A^{-1} and B are bounded. We thus conclude that assumptions $\mathcal{A}\mathbf{1}$, $\mathcal{A}\mathbf{2}$ and $\mathcal{A}\mathbf{3}$ are satisfied.

Recall that, in each iteration of the PDAS method, we must solve the system (35). We will now explore the form of this system for the present model problem. In (35),

$$B^{\mathcal{I}^k} = BE^{\mathcal{I}^k},$$

see the discussion leading to (27). In the present context, we may use (50) to write this operator on the form

$$\begin{aligned} B^{\mathcal{I}^k} &= R_U^{-1}\widehat{B}E^{\mathcal{I}^k} \\ &= R_U^{-1}\widehat{B}^{\mathcal{I}^k}, \end{aligned} \tag{51}$$

where we define

$$\widehat{B}^{\mathcal{I}^k} = \widehat{B}E^{\mathcal{I}^k}.$$

Equation (35) also involves the adjoint operators A^* and $[B^{\mathcal{I}^k}]^*$ of A and $B^{\mathcal{I}^k}$. According to a rather technical argument presented in [11],

$$A^* = R_U^{-1}\widehat{A}', \tag{52}$$

$$[B^{\mathcal{I}^k}]^* = [R_{L^2(\mathcal{I}^k)}]^{-1}[\widehat{B}^{\mathcal{I}^k}]', \tag{53}$$

where the "$'$" notation is used to denote dual operators, and $R_{L^2(\mathcal{I}^k)}$ is the Riesz map of $L^2(\mathcal{I}^k)$ to its dual space, see (16).

From (49), (51), (52) and (53) it follows that the operator $\mathcal{B}_\alpha^k$ in (35) can be written on the form

$$\begin{aligned} \mathcal{B}_\alpha^k &= \begin{bmatrix} \alpha I^{\mathcal{I}^k} & 0 & [B^{\mathcal{I}^k}]^* \\ 0 & T^*T & A^* \\ B^{\mathcal{I}^k} & A & 0 \end{bmatrix} \\ &= \begin{bmatrix} \alpha I^{\mathcal{I}^k} & 0 & [R_{L^2(\mathcal{I}^k)}]^{-1}[\widehat{B}^{\mathcal{I}^k}]' \\ 0 & T^*T & R_U^{-1}\widehat{A}' \\ R_U^{-1}\widehat{B}^{\mathcal{I}^k} & R_U^{-1}\widehat{A} & 0 \end{bmatrix} \\ &= \underbrace{\begin{bmatrix} [R_{L^2(\mathcal{I}^k)}]^{-1} & 0 & 0 \\ 0 & R_U^{-1} & 0 \\ 0 & 0 & R_U^{-1} \end{bmatrix}}_{=[\mathcal{R}^k]^{-1}} \underbrace{\begin{bmatrix} \alpha R_{L^2(\mathcal{I}^k)} & 0 & [\widehat{B}^{\mathcal{I}^k}]' \\ 0 & R_U T^*T & \widehat{A}' \\ \widehat{B}^{\mathcal{I}^k} & \widehat{A} & 0 \end{bmatrix}}_{=\widehat{\mathcal{B}}_\alpha^k}. \end{aligned} \tag{54}$$

We can therefore express

$$\mathcal{B}_\alpha^k p^k = b,$$

cf. (35), appearing in each iteration of the PDAS algorithm, as

$$\begin{bmatrix} [R_{L^2(\mathcal{I}^k)}]^{-1} & 0 & 0 \\ 0 & R_U^{-1} & 0 \\ 0 & 0 & R_U^{-1} \end{bmatrix} \begin{bmatrix} \alpha R_{L^2(\mathcal{I}^k)} & 0 & [\widehat{B}^{\mathcal{I}^k}]' \\ 0 & R_U T^* T & \widehat{A}' \\ \widehat{B}^{\mathcal{I}^k} & \widehat{A} & 0 \end{bmatrix} \begin{bmatrix} v^{\mathcal{I}^k} \\ u^k \\ w^k \end{bmatrix}$$
$$= \begin{bmatrix} [R_{L^2(\mathcal{I}^k)}]^{-1} & 0 & 0 \\ 0 & R_U^{-1} & 0 \\ 0 & 0 & R_U^{-1} \end{bmatrix} \begin{bmatrix} 0 \\ R_U T^* d \\ 0 \end{bmatrix}. \qquad (55)$$

Written more compactly, this system reads

$$[\mathcal{R}^k]^{-1} \widehat{\mathcal{B}}_\alpha^k p^k = [\mathcal{R}^k]^{-1} \widehat{b}, \qquad (56)$$

where

$$\widehat{b} = \mathcal{R}^k b = \begin{bmatrix} 0 \\ R_U T^* d \\ 0 \end{bmatrix},$$
$$p^k = \begin{bmatrix} v^{\mathcal{I}^k} \\ u^k \\ w^k \end{bmatrix}.$$

Note that

$$\widehat{\mathcal{B}}_\alpha^k : L^2(\mathcal{I}^k) \times U \times U \to \left(L^2(\mathcal{I}^k) \times U \times U \right)',$$

and that

$$[\mathcal{R}^k]^{-1} : \left(L^2(\mathcal{I}^k) \times U \times U \right)' \to L^2(\mathcal{I}^k) \times U \times U.$$

One may therefore regard $[\mathcal{R}^k]^{-1}$ to be a preconditioner for the (continuous) KKT system arising in each iteration of the PDAS method applied to (42)-(45), see [9] for further details. Note that the operators $\mathcal{R}^k$, $[\mathcal{R}^k]^{-1}$, $\widehat{\mathcal{B}}_\alpha^k$ and $[\widehat{\mathcal{B}}_\alpha^k]^{-1}$ are bounded. Hence, a proper discretization of these mappings should yield a discretized approximation of (54) which is well behaved for any mesh parameter $h > 0$. This completes the discussion of issue (a).

7.2 Discretization

Let us turn our attention towards the discretization matter mentioned in (b), i.e. the discretization of (56). Recall that $\mathcal{B}_\alpha^k = [\mathcal{R}^k]^{-1} \widehat{\mathcal{B}}_\alpha^k$ only operates on the inactive part of the control. Expressed with mathematical symbols,

$$\mathcal{B}_\alpha^k : L^2(\mathcal{I}^k) \times U \times U \to L^2(\mathcal{I}^k) \times U \times U.$$

Hence, in each iteration of the PDAS method one may regard $L^2(\mathcal{I}^k)$ to be the control space, while the state space U and the observation space Z are defined in (46)-(47), respectively.

As mentioned earlier, one may think of the inverse Riesz maps $[R_{L^2(\mathcal{I}^k)}]^{-1}$ and R_U^{-1}, see (54), as preconditioners. Since $U = H^1(\Omega)$, it follows that, in a FEM setting,

- $R_{L^2(\mathcal{I}^k)}$ "corresponds" to the mass matrix $M_v^{\mathcal{I}^k,\mathcal{I}^k}$ associated with the inactive set $\mathcal{I}^k \subset \Omega_v$,
- R_U "corresponds" to the sum of the mass matrix M and the stiffness matrix S associated with the domain Ω.

Concerning the details of the discretization of the operators in $\widehat{\mathcal{B}}_\alpha^k$, defined in (54), we refer to [9]. If we use the superscript notation "$\mathcal{I}^k$" and " : " to denote the inactive indices and all the indices, respectively, the end result is as follows:

- $\widehat{A}$ yields the matrix $M + S$, which is the sum of the mass and stiffness matrix associated with the domain Ω.
- $\widehat{B}^{\mathcal{I}^k}$ yields the matrix $M_v^{\mathcal{I}^k,:}$, where M_v is the mass matrix associated with the sub domain Ω_v of Ω.
- $R_U T^* T$ yields the matrix M_∂, which is the mass matrix associated with the boundary $\partial\Omega$ of the domain Ω.
- The functions v, u, w and d yields the corresponding vectors $\bar{v}$, $\bar{u}$, $\bar{w}$ and $\bar{d}$.

Hence, the discretized system associated with (55) reads

$$\begin{bmatrix} M_v^{\mathcal{I}^k,\mathcal{I}^k} & 0 & 0 \\ 0 & M+S & 0 \\ 0 & 0 & M+S \end{bmatrix}^{-1} \underbrace{\begin{bmatrix} \alpha M_v^{\mathcal{I}^k,\mathcal{I}^k} & 0 & M_v^{\mathcal{I}^k,:} \\ 0 & M_\partial & M+S \\ M_v^{:,\mathcal{I}^k} & M+S & 0 \end{bmatrix}}_{\bar{\mathcal{B}}_\alpha^k} \underbrace{\begin{bmatrix} \bar{v}^{\mathcal{I}^k} \\ \bar{u}^k \\ \bar{w}^k \end{bmatrix}}_{\bar{p}^k}$$
$$= \begin{bmatrix} M_v^{\mathcal{I}^k,\mathcal{I}^k} & 0 & 0 \\ 0 & M+S & 0 \\ 0 & 0 & M+S \end{bmatrix}^{-1} \underbrace{\begin{bmatrix} 0 \\ M_\partial \bar{d} \\ 0 \end{bmatrix}}_{\bar{b}}. \tag{57}$$

We thus use the preconditioner

$$[\bar{\mathcal{R}}^k]^{-1} = \begin{bmatrix} M_v^{\mathcal{I}^k,\mathcal{I}^k} & 0 & 0 \\ 0 & M+S & 0 \\ 0 & 0 & M+S \end{bmatrix}^{-1}. \tag{58}$$

We have now handled both issues (a) and (b), and derived a discretized preconditioned KKT system (57). It remains to discretize the Lagrange multiplier update (36). Since the procedure for doing this is very similar to the discussion of the KKT system, we leave the technical details to Appendix A. The end result is the update

$$M_v^{\mathcal{A}^k,\mathcal{A}^k}\bar{\lambda}^{\mathcal{A}^k} = M^{\mathcal{A}^k,:}\bar{w}^k, \tag{59}$$

where " $\mathcal{A}^k$ " denotes the active indices.

To summarize, in each iteration of the PDAS algorithm we must solve the preconditioned system (57). The Lagrange multiplier $\bar{\lambda}^{\mathcal{A}^k}$ is thereafter computed by solving (59). Finally, the active and inactive sets are updated according to steps 9 and 10 in Algorithm 1.

7.3 Numerical setup

- All code was written in the framework of cbc.block, which is a FEniCS-based Python implemented library for block operators. See [8] for a full description of cbc.block.

- We used the PyTrilinos package to compute an approximation of the preconditioner (58), using algebraic multigrid (AMG) with a symmetric Gauss-Seidel smoother and three smoothing sweeps. All tables containing iteration counts for the MINRES method were generated with this approximate inverse Riesz map. On the other hand, the eigenvalues of the KKT systems $[\bar{\mathcal{R}}^k]^{-1}\bar{\mathcal{B}}_\alpha^k$, see (57)-(58), were computed with an *exact* inverse $[\bar{\mathcal{R}}^k]^{-1}$ computed in Octave.

- We divided the domain of $\Omega = (0,1)\times(0,1)$ into $N \times N$ squares, and each of these squares were divided into two triangles.

- The following stopping criterion was used to stop the MINRES iteration process

$$\frac{\|r_n^k\|}{\|r_0^k\|} = \left[\frac{(\ \bar{\mathcal{B}}_\alpha^k\bar{p}_n^k - \bar{b}, [\bar{\mathcal{R}}^k]^{-1}[\bar{\mathcal{B}}_\alpha^k\bar{p}_n^k - \bar{b}]\ )}{(\ \bar{\mathcal{B}}_\alpha^k\bar{p}_0^k - \bar{b}, [\bar{\mathcal{R}}^k]^{-1}[\bar{\mathcal{B}}_\alpha^k\bar{p}_0^k - \bar{b}]\ )}\right]^{1/2} < \epsilon, \tag{60}$$

  where ϵ is a small positive parameter. Note that the superindex k is the iteration index for the "outer" PDAS method, while the subindex n is the iteration index for the "inner" MINRES algorithm at each step of the PDAS method.

- In the synthetic examples no noise was added to the input data d, see (1). For the problem involving real world data, however, the input data was given by clinical recordings and obviously contained a significantly amount of noise.

- Synthetic observation data d, used in (42), was produced by setting

$$v(x) = 3\sin(2\pi x_1), x = (x_1, x_2) \in \Omega_v, \tag{61}$$

in (43). Thereafter the boundary value problem (43)-(44) was solved and d was put equal to $u|_{\partial\Omega}$. Note that the control (61) cannot be recovered by solving the optimality system (42)-(45), due to the inequality constraint $v(x) \geq 0$. Hence, the problem formulation might seem peculiar, but as the goal of this example is to study the iteration numbers for the reduced KKT systems, it is desirable to have active constraints for all reasonable values of the regularization parameter α. An experimental investigation suggested the use of a control function of the form (61) to obtain nonempty active sets for large values of the regularization parameter α ($\alpha \approx 1$).

7.4 Results

We are now ready to proceed to the actual experiments. In the introduction we mentioned that the KKT system associated with (1)-(2), without box constraints, has a spectrum of the form (5), as long as assumptions $\mathcal{A}\mathbf{1}$-$\mathcal{A}\mathbf{5}$ in Section 2 are fulfilled. Recall that Theorem 6.3 asserts that such a spectrum will be inherited by each subsystem in the PDAS algorithm, provided that assumption $\mathcal{A}\mathbf{5}$ still holds. Figure 1 shows the spectrum of such a subsystem. It is definitely on the form (40), and we expect that the MINRES method will solve the KKT systems efficiently.

Table 1 contains the average number of MINRES iterations required to solve the reduced KKT systems. That is, the average number of MINRES iterations needed in each iteration of the PDAS algorithm. In these experiments we used a zero initial guess in every run of the MINRES method, i.e. $\bar{p}_0^k = 0$, see (60).

In [11] the authors proved that the number of required MINRES iterations cannot grow faster than $O([\ln(\alpha^{-1})]^2)$, and also explained why iterations counts of order $O([\ln(\alpha^{-1})])$ often will occur in practice. Consider the last row of Table 1, i.e. $N = 512$. For the stopping criterion $\epsilon = 10^{-6}$ in (60), the iteration counts can be relatively well modeled by the formula

$$32.2 - 10.5\log_{10}(\alpha),$$

where we used the method of least squares to estimate the constants in this expression. Similarly, for $N = 512$ and the stopping criterion $\epsilon = 10^{-10}$, we can model the work effort rather accurately with the formula

$$45.0 - 20.1\log_{10}(\alpha).$$

We conclude that the required number of MINRES iteration only grows (approximately) logarithmically as the regularization parameter $\alpha \to 0$.

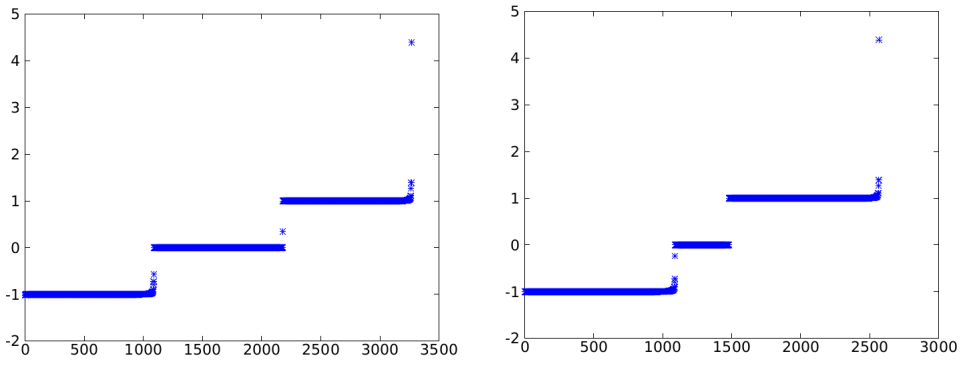

a) b)

Figure 1: The eigenvalues of $[\bar{\mathcal{R}}^k]^{-1}\bar{\mathcal{B}}^k_\alpha$ in Example 1. Panel a) displays the eigenvalues of the full system, i.e. no active constraints and $\mathcal{I}^k = \Omega_v$. Furthermore, $\alpha = 0.0001$ and $N = 32$. Panel b) shows the spectrum of a reduced KKT system, with 700 active inequalities. We observe that there are fewer eigenvalues in the interval $[c\alpha, 2\alpha]$ in panel b), cf. (40)). More specifically, 700 eigenvalues have been "removed" from this interval in panel b), compared with panel a). We do not present a plot of the isolated eigenvalues, i.e. $\lambda_i \in (2\alpha, a)$, since the full system only has three isolated eigenvalues, and the reduced system only has one isolated eigenvalue.

Note that the spectral condition number $\kappa(\mathcal{B}^{k,h}_\alpha)$ of $\mathcal{B}^{k,h}_\alpha$ is of order $O(\alpha^{-1})$, which is "confirmed" by Figure 1. The standard theory for Krylov subspace solvers states that MINRES needs $O(\kappa(\mathcal{B}^{k,h}_\alpha))$ iterations. Hence, the classical estimate provides a very pessimistic estimate for the needed workload.

Table 1 contains iteration counts for both $\epsilon = 10^{-6}$ and $\epsilon = 10^{-10}$, cf. the stopping condition (60). We observe that the iteration numbers increase roughly by a factor of 1.5 if ϵ is decreased from 10^{-6} to 10^{-10}. However, we see no visible difference between the controls v_1 and v_2 computed with these two stopping criteria, see Figure 2. In fact, the relative difference between the solutions depicted in this figure is $2.12 * 10^{-5}$. In retrospect, we conclude that the choice $\epsilon = 10^{-10}$ does not significantly increase the accuracy of the solution compared to the choice $\epsilon = 10^{-6}$. Thus, choosing a suitable stopping criterion is a delicate matter; the criterion must be strict enough to obtain convergence, but not so hard that many unnecessary iterations are performed.

We have previously mentioned that the experiments presented in Table 1 were performed using the zero initial guess in every run of the MINRES method, i.e. $\bar{p}^k_0 = 0$. Intuitively, the initial guess $\bar{p}^k_0 = \bar{p}^{k-1}_n$ might seem

N\α	1	.1	.01	.001	.0001
32	23	32	38	46	56
64	27	36	42	51	66
128	27	37	42	52	71
256	33	42	48	59	75
512	33	44	52	59	78

(a) Stopping criterion $\epsilon = 10^{-6}$.

N\α	1	.1	.01	.001	.0001
32	34	45	55	70	86
64	39	52	64	83	103
128	41	54	67	85	109
256	48	61	75	95	121
512	49	64	80	103	130

(b) Stopping criterion $\epsilon = 10^{-10}$.

Table 1: The average number of MINRES iterations required to solve the reduced KKT systems in the PDAS algorithm. The two panels display the iteration counts for two different choices of ϵ, see (60). Here, we used the initial guess $\bar{p}_0^k = 0$ in the MINRES algorithm for iteration k of the PDAS method.

preferable. That is, we set the initial guess for the MINRES algorithm equal to the solution from the previous PDAS iteration. In this case, however, (60) should be adjusted to avoid an unreasonable strict stopping criterion when $\bar{p}_n^{k-1} \approx \bar{p}^*$, where $\bar{p}^*$ is the exact solution of the discretized PDE constrained optimization problem. We suggest the following alternative stopping criterion to terminate the MINRES iteration process:

$$\frac{\|r_n^k\|}{\|r_0^0\|} = \left[\frac{(\ \bar{\mathcal{B}}_\alpha^k \bar{p}_n^k - \bar{b}, [\bar{\mathcal{R}}^k]^{-1}[\bar{\mathcal{B}}_\alpha^k \bar{p}_n^k - \bar{b}]\ )}{(\ \bar{\mathcal{B}}_\alpha^0 \bar{p}_0^0 - \bar{b}, [\bar{\mathcal{R}}^0]^{-1}[\bar{\mathcal{B}}_\alpha^0 \bar{p}_0^0 - \bar{b}]\ )} \right]^{1/2} < \epsilon. \tag{62}$$

Note that the initial guess $\bar{p}_0^k = \bar{p}_n^{k-1}$ and the alternative stopping criterion (62) will consistently be used together. Similarly, when we employ the initial guess $\bar{p}_0^k = 0$, the criterion (60) will be used to terminate the iteration process.

How these two different initial guesses affect the iteration counts, can be observed by comparing Table 1 with Table 2. In Table 1 we used the initial guess $\bar{p}_0^k = 0$ in every run of the MINRES method, whereas for the numbers presented in Table 2 we employed $\bar{p}_0^k = \bar{p}_n^{k-1}$. For large values of α, we observe a reduction in the iteration counts, but this effect seems to be less apparent for the smaller values of α. We suspect this to be linked to our choice of synthetic observation data, d, which was generated by the control (61). For this observation data d, and small values of α, the solutions of (42)-(44) and (42)-(45) are very different, i.e. the inequality constraints have a significant impact. As a result of this difference, the initial guess $\bar{p}_0^k = \bar{p}_n^{k-1}$ is not much better than the zero guess. We will return to this matter in the next section.

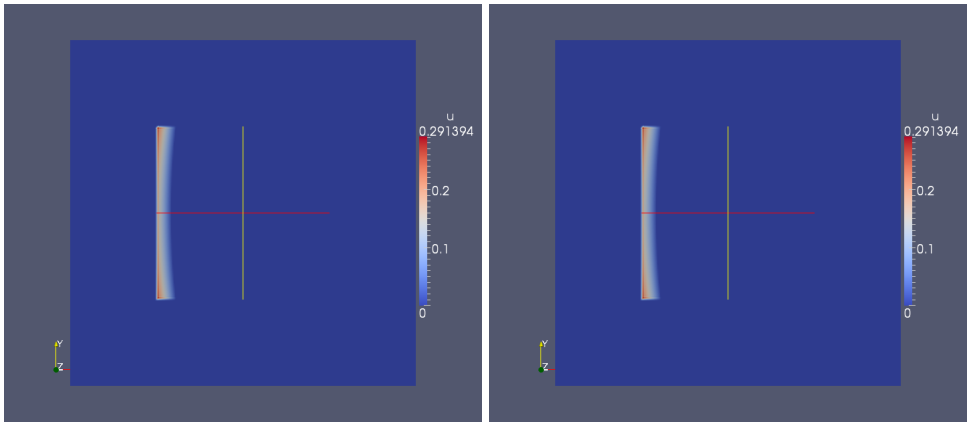

(a) Stopping criterion $\epsilon = 10^{-6}$. (b) Stopping criterion $\epsilon = 10^{-10}$.

Figure 2: The solution of (42)-(45) for two different stopping criteria. In these examples, $N = 256$ and $\alpha = 0.01$. The relative difference $\frac{\|v_1 - v_2\|_{L^2(\Omega)}}{\|v_1\|_{L^2(\Omega)}}$ between these two control functions is $2.12 * 10^{-5}$.

8 The inverse problem of electrocardiography

We will now study a real world problem. In the *inverse problem of electrocardiography* one attempts to identify an ischemic region/infarction by combining ECG recordings with the, so called, bidomain model [2]. Since the derivation of the bidomain model is not essential for understanding the optimization problem, we refer to [13] for further details about this model.

The control function v in this application, however, must be addressed in some detail. In this medical problem, the control v is the transmembrane potential of the heart, i.e. the potential difference over the cell membrane of the heart cells. According to biomedical knowledge, we know *a priori* that this potential satisfies

$$v(x) \approx \begin{cases} 0mV & x \text{ in healthy tissue,} \\ 50mV & x \text{ in ischemic tissue.} \end{cases} \tag{63}$$

Our objective is to compute the transmembrane potential v by solving an optimization problem. Thereafter, we use (63) to determine the ischemic region, i.e. this region is the sub-domain of the heart where $v(x) \approx 50$.

The optimization problem will be related to the form (1)-(3), where we have the following information:

- The input data d in (1) is a normalized clinical ECG recording.

[2] Ischemia is a state of reduced blood supply to the heart, usually due to coronary artery disease. It is a reversible condition, but also a precursor to a full heart attack.

N\α	1	.1	.01	.001	.0001
32	16	14	36	46	54
64	15	28	36	50	65
128	13	22	31	46	64
256	15	26	35	49	68
512	15	23	36	51	69

(a) Stopping criterion $\epsilon = 10^{-6}$.

N\α	1	.1	.01	.001	.0001
32	27	32	51	70	85
64	25	46	58	80	102
128	27	35	60	80	105
256	32	40	62	79	103
512	25	46	64	90	109

(b) Stopping criterion $\epsilon = 10^{-10}$.

Table 2: The average number of MINRES iterations required to solve the reduced KKT systems in the PDAS algorithm. The two tables contain the iteration counts for two different choices of ϵ, see (62). Here, we used the initial guess $\bar{p}_0^k = \bar{p}_n^{k-1}$ in the MINRES algorithm for iteration k of the PDAS method.

- The state equation (2) will be the bidomain model[3].
- We use (63) to define suitable inequality constraints.
- The *control space*, however, is no longer an L^2-space, but an H^1-space.

In detail, the optimization problem can be formulated as follows

$$\min_{(v,u)\in H^1(\Omega_H)\times H^1(\Omega_B)} \left\{ \frac{1}{2}\|Tu - d\|^2_{L^2(\partial\Omega_B)} + \frac{1}{2}\alpha\|v\|^2_{H^1(\Omega_H)} \right\} \tag{64}$$

subject to

$$\int_{\Omega_B} \nabla\psi \cdot M\nabla u \, dx = -\int_{\Omega_H} \nabla\psi \cdot M_i\nabla v \, dx, \ \forall\psi \in X, \tag{65}$$

$$v(x) \geq 0, \ x \in \Omega_H, \tag{66}$$

where

$$M(x) \approx \begin{cases} M_i(x) + M_e(x), & x \in \Omega_H, \\ M_o(x), & x \in \Omega_T. \end{cases}$$

Remark 8.1. *Note that (63) also implies an upper bound for v. This upper bound, however, is dependent on a number of model parameters and is, for reasons outside the scope of this article, not as essential as the lower bound. In addition, our simulations did not provoke any active upper constraints.*

In this section we use the following notation:

· v is the transmembrane potential.

[3]As in Example 1, the bidomain equation involves an operator $\hat{A}$ mapping U onto its dual space U'. Hence, we need an inverse Riesz map to obtain a minimization problem of the form (1)-(3).

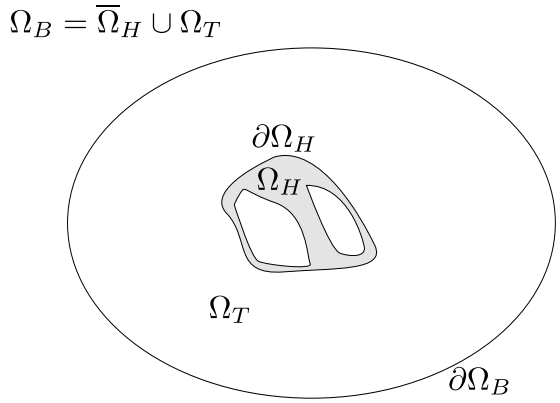

Figure 3: A 2D picture of the domains. Ω_H represents the heart and is depicted in gray color. We denote the remaining domain by the torso, Ω_T. The cavities (white areas) inside the heart represent the ventricles.

- u is the extracellular potential.
- d_{raw} is the ECG recording, and $d = d_{\text{raw}} - \frac{1}{|\partial\Omega_B|}\int_{\partial\Omega_B} d_{\text{raw}}$ is a normalization of the data with respect to the boundary integral, see [10] for details.
- M_i and M_e are the intracellular and extracellular conductivity tensors of the heart, respectively.
- M_o is the extracellular conductivity of the torso.
- Ω_H is the domain of the heart.
- Ω_T is the domain of the torso.
- $\Omega_B = \overline{\Omega}_H \cup \Omega_T$ is the domain of the body.
- $U = \{q \in H^1(\Omega_B) : \int_{\partial\Omega_B} q = 0\}$. Reasons for using this particular Hilbert space are discussed in [10].

For a visual representation of the domains Ω_H, Ω_T and Ω_B, see Figure 3.

Remark 8.2. *In this example, the control space is no longer $L^2(\Omega_v)$, but $H^1(\Omega_H)$, which is not covered by the analysis presented in the theoretical sections. To derive a PDAS algorithm for this H^1-framework is, to the authors knowledge, still an open challenge. Essentially, the problem is that the inequality conditions can no longer be expressed on the simple explicit form* (7)-(8)*, but instead involve solving an obstacle problem, see [6] for further details.*

For a strictly finite dimensional optimization problem, however, a PDAS algorithm exists. Unfortunately, we can then no longer guarantee that it will reflect the structure of the associated infinite dimensional problem. Nevertheless, we find it interesting to investigate the problem from a practical point of view.

Since the discretization of the optimality system associated with (64)-(66) is almost identical to the discretization of the optimality system in Example 1, we will first present the results and thereafter return to the mathematical treatment of (64)-(66).

For the simulations, we have two different sets of patient data, both recorded at Oslo University Hospital. For each of the two patients, we have patient specific geometrical models. Figure 4 shows the body mesh associated with Patient 1. Note that the grid is highly unstructured.

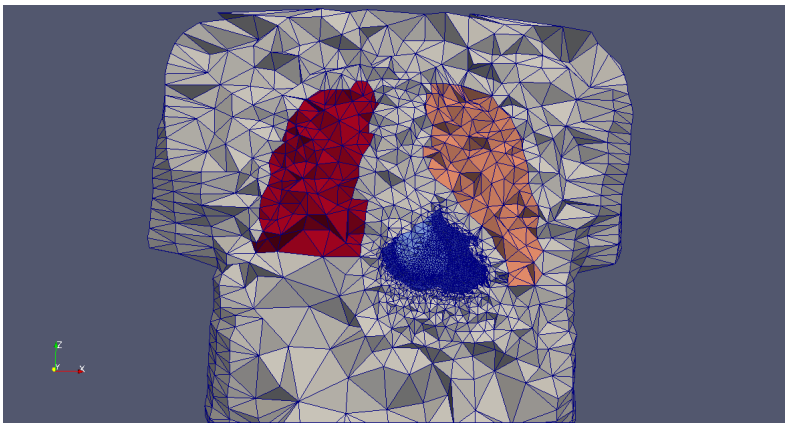

Figure 4: The body mesh associated with Patient 1. The blue color represents the heart, and the red colors represent the lungs. The mesh consists of $51,489$ nodes, whereof 33,156 are located in the heart.

8.1 Results

Table 3 and Table 4 contains the iteration counts for Patient 1 and Patient 2, respectively. The numbers are much higher than those reported for the synthetic example (Example 1), but the growth is still (approximately) logarithmic as $\alpha \to 0$. For Patient 1 the iteration counts for $k = 0$, i.e. the first PDAS iteration, can be modeled by the formula

$$2064.6 - 1287.6 \log_{10}(\alpha).$$

Similarly, we can model the average workload for Patient 1 by the formula

$$1225 - 798.4 \log_{10}(\alpha).$$

We would like to stress that, in this example, the relatively high iteration numbers do not appear to be linked to the fact that our control space is H^1, instead of L^2. More precisely, the iteration counts for $k = 0$, i.e. when there are *no* active constraints, are not lower than for $k > 0$. Other possible explanations for the high iteration numbers will be discussed in Section 9.

For this real world application, we are not only interested in the iteration counts, but also in the actual time it takes to solve the optimization problem. All simulations were performed on a regular laptop with the *Intel®Core^{TM}i5-2520M CPU @ 2.50GHz × 4* processor. From Table 3, we conclude that it lasted between 5 and 13 minutes to solve the inequality constrained optimization problem for Patient 1. For Patient 2, it took between 6 and 15 minutes, depending on the choice of α. For the particular choice of regularization parameter $\alpha = 0.1$, 664 seconds were required. The computed control function for this choice of α can be seen in Figure 5. The figure also displays the solution of (64)-(65), i.e. the optimization problem without the inequality constraint. We see that the introduction of (66) sharpens the image, and thus provides a more well defined separation of the ischemic region and the healthy tissue. For the cardiologists, such a clear distinction is definitely desirable. In fact, one may argue that the image computed without box constraints is of no practical value.

$k\backslash\alpha$	1	$10^{-1/2}$	10^{-1}	$10^{-3/2}$	10^{-2}
0	1808	2851	3694	3911	4497
1	1127	1480	1967	2281	2426
2	361	741	880	1046	1279
Mean	1099	1691	2180	2413	2734
Wall Time	308s	467s	598s	659s	770s

Table 3: The wall time and the number of MINRES iterations required to solve the optimization problem for Patient 1. Note that k denotes the PDAS iteration number. Here, the stopping criterion was $\epsilon = 10^{-6}$, see (62).

$k\backslash\alpha$	1	$10^{-1/2}$	10^{-1}	$10^{-3/2}$	10^{-2}
0	1879	2977	3224	4080	4717
1	1332	1747	2499	2751	3256
2	608	1032	1403	2005	2233
Mean	1273	1919	2375	2945	3402
Wall Time	362s	538s	664s	794s	909s

Table 4: The wall time and the number of MINRES iterations required to solve the optimization problem for Patient 2. Note that k denotes the PDAS iteration number. Here, the stopping criterion was $\epsilon = 10^{-6}$, see (62).

$k\backslash\alpha$	1	$10^{-1/2}$	10^{-1}	$10^{-3/2}$	10^{-2}
Mean	1488	2111	2821	3027	3408
Wall Time	400s	586s	761s	810s	902s

Table 5: The wall time and the average number of MINRES iterations required to solve the optimization problem for Patient 1. These numbers were generated with the initial guess $\bar{p}_0^k = 0$ in every run of the MINRES method, and the stopping criterion was $\epsilon = 10^{-6}$, see (60).

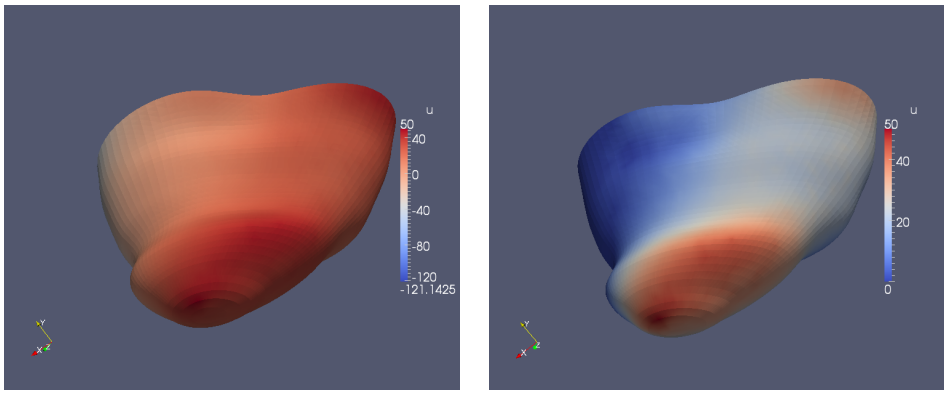

(a) Inverse solution *without* inequality constraints.

(b) Inverse solution *with* inequality constraints.

Figure 5: The computed transmembrane potential v for Patient 2. Here, $\alpha = 0.1$. Panel a) shows the solution of (64)-(65). Panel b), on the other hand, displays the solution of the full problem (64)-(66).

Recall that we, in Example 1, discussed the effect of the initial guess on the performance of the MINRES algorithm. In the present real world application, we have so far reported results obtained with the initial guess $\bar{p}_0^k = \bar{p}_n^{k-1}$. For reason of comparison, we also ran simulations with $\bar{p}_0^k = 0$, see (60). The iteration counts and wall time obtained for these computations can be found in Table 5. Contrary to what was observed in Example 1, we conclude that the initial guess $\bar{p}_0^k = \bar{p}_n^{k-1}$ yields a significant improvement, compared with the "naive" guess $\bar{p}_0^k = 0$. We save roughly $400 - 600$ iterations on average. From a computing-time perspective, the reduction is also significant, with savings in the range of 90 seconds to 3 minutes, i.e. about a 20% reduction in computing-time.

8.2 Discretization

We now return to the mathematical aspects of (64)-(66). Note that the control space V, the state space U and the observation space Z are

$$\begin{aligned} V &= H^1(\Omega_H), \\ U &= \left\{ q \in H^1(\Omega_B) : \int_{\partial\Omega_B} q = 0 \right\}, \\ Z &= L^2(\partial\Omega_B), \end{aligned}$$

see Figure 3 for an overview of the domains. Hence, we are trying to recover a function $v \in H^1(\Omega_H)$ from an observation $d \in L^2(\partial\Omega_B)$ of u along the boundary $\partial\Omega_B$ of the body Ω_B. Notice the form of (63). Since the unknown control is known, a priori, to be approximately piecewise constant, it seems natural to put more weight on the derivative of v in the regularization. Therefore, we use the weighted norm

$$\|v\|_V^2 = \rho\|v\|_{L^2(\Omega_H)}^2 + \|\nabla v\|_{L^2(\Omega_H)}^2$$

on V, where $0 < \rho \ll 1$. This will be reflected in the block operators presented below. In our experiments, we have chosen $\rho = 10^{-4}$.

We start our derivation of the optimality system by considering the state equation (65). This equation can be written as

$$\langle \widehat{A}u, \psi \rangle = -\langle \widehat{B}v, \psi \rangle, \ \forall \psi \in U,$$

where

$$\begin{aligned} \widehat{A} : U \to U', \ \ u \to \int_{\Omega_B} \nabla\psi \cdot M\nabla u \ dx, \psi \in U, \\ \widehat{B} : V \to U', \ \ v \to \int_{\Omega_H} \nabla\psi \cdot M_i\nabla v \ dx, \psi \in U. \end{aligned}$$

We can now proceed as in Example 1 and derive a KKT system with a structure similar to (55). Once more, we refer to [9] for details regarding the matrix representation of the operators in the KKT system. By letting " $\mathcal{I}^k$ " and " : " denote the inactive indices and all indices, respectively, the discretization can roughly be described as follows:

- $R_{V^{\mathcal{I}^k}}$ yields the sum $(\rho M_H + S_H)^{\mathcal{I}^k,\mathcal{I}^k}$ of the mass matrix M_H and the stiffness matrix S_H associated with the domain $\mathcal{I}^k \subset \Omega_H$.
- R_U yields the stiffness matrix S_B associated with the domain Ω_B. [4]

[4] Recall that $U = \{q \in H^1(\Omega_B) : \int_{\partial\Omega_B} q = 0\}$, which makes it possible to use the Poincaré inequality to define the norm $\|\cdot\|_U$ on U as $\|q\|_U = \int_{\Omega_B} |\nabla q|^2$. It therefore follows that the Riesz map only yields the stiffness matrix.

- $\widehat{A}$ yields the matrix N associated with the operator $-\nabla \cdot M\nabla u$ on Ω_B.
- $\widehat{B}$ yields the matrix L associated with the operator $\nabla \cdot M_i \nabla v$ on Ω_H, and consequently, $\widehat{B}^{\mathcal{I}^k}$ yields the matrix $L^{\mathcal{I}^k,:}$.
- $R_U T^* T$ yields the matrix M_∂, which is the mass matrix associated with the boundary $\partial\Omega_B$ of the body Ω_B.

Hence, the discretized KKT system will in this case read:

$$\begin{bmatrix} (\rho M_H + S_H)^{\mathcal{I}^k,\mathcal{I}^k} & 0 & 0 \\ 0 & S_B & 0 \\ 0 & 0 & S_B \end{bmatrix}^{-1} \begin{bmatrix} \alpha(\rho M_H + S_H)^{\mathcal{I}^k,\mathcal{I}^k} & 0 & L^{\mathcal{I}^k,:} \\ 0 & M_\partial & N \\ L^{:,\mathcal{I}^k} & N & 0 \end{bmatrix} \begin{bmatrix} \bar{v}^{\mathcal{I}^k} \\ \bar{u}^k \\ \bar{w}^k \end{bmatrix}$$
$$= \begin{bmatrix} (\rho M_H + S_H)^{\mathcal{I}^k,\mathcal{I}^k} & 0 & 0 \\ 0 & S_B & 0 \\ 0 & 0 & S_B \end{bmatrix}^{-1} \begin{bmatrix} 0 \\ M_\partial \bar{d} \\ 0 \end{bmatrix}.$$

We thus use the preconditioner

$$[\bar{\mathcal{R}}^k]^{-1} = \begin{bmatrix} (\rho M_H + S_H)^{\mathcal{I}^k,\mathcal{I}^k} & 0 & 0 \\ 0 & S_B & 0 \\ 0 & 0 & S_B \end{bmatrix}^{-1}. \tag{67}$$

Finally, we update the Lagrange multiplier $\bar{\lambda}^{\mathcal{A}^k}$ by solving

$$(\rho M_H + S_H)^{\mathcal{A}^k,\mathcal{A}^k} \bar{\lambda}^{\mathcal{A}^k} = L^{\mathcal{A}^k,:} \bar{w}^k,$$

where " $\mathcal{A}^k$ " denotes the active indices. (The derivation of this update is similar to the one leading to (59).

8.3 A $H^1(\Omega_v)$ control space on a regular grid

We have already discussed that the lack of a continuous PDAS algorithm for cases involving a $H^1(\Omega_v)$ control space do not seem to affect the performance of the preconditioner for the inverse ECG problem studied above. Now, we explore this issue further by considering the optimization problem

$$\min_{(v,u)\in H^1(\Omega_v)\times H^1(\Omega)} \left\{ \frac{1}{2}\|Tu - d\|^2_{L^2(\partial\Omega)} + \frac{1}{2}\alpha\|v\|^2_{H^1(\Omega_v)} \right\} \tag{68}$$

subject to

$$\int_\Omega \nabla\psi \cdot \nabla u \, dx + \int_\Omega \psi u \, dx = -\int_{\Omega_v} \nabla\psi \cdot \nabla v \, dx, \ \forall \psi \in H^1(\Omega), \tag{69}$$

$$v(x) \geq 0, \ x \in \Omega_v. \tag{70}$$

The domains Ω and Ω_v are defined as follows:

$$\Omega = (0,1) \times (0,1),$$
$$\Omega_v = \left(\frac{1}{4}, \frac{3}{4}\right) \times \left(\frac{1}{4}, \frac{3}{4}\right).$$

We will not present all the computational details, but instead focus on the iteration numbers for the preconditioned MINRES scheme applied to the KKT system associated with (68)-(70).

$N \backslash k$	0	1
64	237	209
128	273	227
256	297	277
512	334	275
1024	390	351

Table 6: The number of MINRES iterations required to solve the optimization problem (68)-(70). Note that k denotes the PDAS iteration number. For $k = 0$ there are *no* active constraints, whereas for $k = 1$ many constrains are active. Here, the stopping criterion was $\epsilon = 10^{-10}$, see (62), $\alpha = 0.01$, and the initial guess was set to $\bar{p}_0^k = 0$ for each PDAS iteration.

From Table 6 we conclude, at least for this problem, that there are no practical difficulties with combining our preconditioner with the PDAS algorithm. On the contrary, we observe a decrease in the number of MINRES iterations needed for $k = 1$, compared with the results obtained for $k = 0$. Note that, in the first PDAS iteration, i.e. $k = 0$, there are *no* active constraints, whereas for $k = 1$ many constrains are active. Hence, for this problem, the lack of a well defined extension operator $E^{\mathcal{I}^k}$, see (17)-(19), does not seem to introduce any severe difficulties. Nevertheless, further theoretical investigations are needed to develop a robust PDAS algorithm for PDE-constrained optimization problems with $H^1(\Omega_v)$ control spaces.

9 Conclusions

In this article we have analyzed the KKT systems arising in each iteration of the PDAS algorithm applied to PDE-constrained optimization problems with box constraints. More specifically, we have investigated whether the system

$$\mathcal{B}_\alpha^k p^k = b$$

can be solved efficiently with the MINRES method. Here, α is the Tikhonov regularization parameter, and $\mathcal{B}_\alpha^k$ denotes the indefinite Hermitian operator arising in each iteration of the PDAS scheme.

Our main theoretical result shows that the discretized operator $\mathcal{B}_\alpha^{k,h}$, associated with $\mathcal{B}_\alpha^k$, has a spectrum with a very limited number $N(\alpha)$ of isolated eigenvalues, whereas the remaining eigenvalues are contained in three bounded intervals:

$$\mathrm{sp}(\mathcal{B}_\alpha^{k,h}) \subset [-b,-a] \cup [c\alpha, 2\alpha] \cup \{\lambda_1, \lambda_2, ..., \lambda_{N(\alpha)}\} \cup [a,b]. \tag{71}$$

For severely ill-posed problems $N(\alpha) = O(\ln(\alpha^{-1}))$. Theoretically, we therefore conclude that the MINRES algorithm will solve the KKT systems efficiently. Furthermore, since the spectral condition number $\kappa(\mathcal{B}_\alpha^{k,h})$ of $\mathcal{B}_\alpha^{k,h}$ is of order $O(\alpha^{-1})$, and the standard theory for the MINRES method states that $O(\kappa(\mathcal{B}_\alpha^{k,h}))$ iterations are required, we conclude that the classical analysis provides a pessimistic estimate for the needed workload.

In [11] it was established that the spectrum of the KKT system associated with (1)-(2), without inequality constraints, is on the form (71). From a technical point of view, the main challenge addressed in this paper was to prove that this property is inherited by the KKT system arising in each iteration of the PDAS method.

We presented a number of numerical experiments. In the first synthetic example, Example 1, we were interested in the growth of the iteration numbers with respect to both the regularization parameter α and the mesh parameter h. For the parameter α, we observed iteration counts almost of order

$$O(\ln(\alpha^{-1}))$$

as $\alpha \to 0$. Moreover, tables 1 and 2 show that the algorithm is robust with respect to the mesh parameter h. Theoretically, the spectral condition numbers of the KKT systems are bounded independently of any $h > 0$, and the slight increase we observed in practice is probably due to computational issues with the algebraic multigrid scheme.

In Section 8 we presented results for a real world problem. Namely, the *inverse problem of electrocardiography (ECG)* in which the unknown source is an ischemic region in the heart. Also for this problem, iteration counts approximately of order $O(\ln(\alpha^{-1}))$ were obtained. The numbers were, however, much higher than the iteration counts encountered in Example 1. This can be due to a number of reasons: The size of the domain, the unstructured grid, the noise in the data, or the form of the state equations. All these issues should be investigated properly in a separate paper.

Neither the inverse ECG problem, nor the synthetic example considered in Section 8.3, fulfill all the assumptions needed by our theoretical analysis. More specifically, these examples involve an H^1 control space, such that suitable extension operators, needed by the PDAS scheme, are not readily available. Nevertheless, our experiments revealed that solving the associated KKT systems, with many active constraints, did not require more MINRES iterations than solving unconstrained problems. Also, we obtained a rather

limited growth in the iteration numbers, as α decreased, for the real world application. In fact, we solved this problem in roughly 5 to 15 minutes, depending on the value of regularization parameter α. With optimized preconditioners, code optimization and a stronger CPU, it should be possible to reduce the computing time to less than 1 minute. For example, by changing the preconditioner (67) to

$$[\mathcal{R}^k]^{-1} = \begin{bmatrix} (\rho M_H + S_H)^{\mathcal{I}^k,\mathcal{I}^k} & 0 & 0 \\ 0 & N & 0 \\ 0 & 0 & N \end{bmatrix}^{-1}, \tag{72}$$

we get iteration counts as reported in Table 7. Clearly, substituting the stiffness matrix S_B in (67) with the matrix N, associated with the operator $-\nabla \cdot M\nabla$ on Ω_B, reduces the iteration counts and computing time significantly.

$k\backslash\alpha$	1	$10^{-1/2}$	10^{-1}	$10^{-3/2}$	10^{-2}
0	993	1528	2194	2661	3085
1	621	953	1224	1622	1715
2	191	444	693	817	948
Mean	602	975	1370	1700	1916
Wall Time	177s	285s	390s	471s	518s

Table 7: The number of MINRES iterations required to solve the optimization problem for Patient 1. These numbers were generated with the alternative preconditioner (72). Note that k denotes the PDAS iteration number. Here, the stopping criterion was $\epsilon = 10^{-6}$, see (62).

The overall conclusion of this paper is: By combining the MINRES method and the PDAS algorithm, some PDE constrained optimization problems arising in real world applications can be solved within reasonable time limits.

Acknowledgements

The authors would like to express their sincere gratitude to the FEniCS community. In particular we would like to thank Kent-André Mardal and Martin Sandve Alnæs for their contribution to the code development. We would also like to thank Kristina Hermann Haugaa, Andreas Abildgaard and Jan Gunnar Fjeld at Oslo University Hospital and Simula Research Laboratory for providing the clinical data used in this study.

A

We will discretize the update of the Lagrange multiplier in Example 1, see the discussion preceding (59). The generic update for this multiplier is given in (36) as

$$\lambda^{\mathcal{A}^k} = [B^{\mathcal{A}^k}]^* w^k, \tag{73}$$

where in each iteration of the PDAS method

$$B^{\mathcal{A}^k} = BE^{\mathcal{A}^k},$$

see (28). Furthermore, recall from (50) that

$$B = R_U^{-1}\widehat{B}.$$

It then follows from (28) that

$$\begin{aligned} B^{\mathcal{A}^k} &= R_U^{-1}\widehat{B}E^{\mathcal{A}^k} \\ &= R_U^{-1}\widehat{B}^{\mathcal{A}^k}, \end{aligned}$$

where

$$\widehat{B}^{\mathcal{A}^k} = \widehat{B}E^{\mathcal{A}^k}.$$

The update (73) involves the adjoint operator $[B^{\mathcal{A}^k}]^*$ of $B^{\mathcal{A}^k}$. According to a rather technical argument presented in [11],

$$[B^{\mathcal{A}^k}]^* = [R_{L^2(\mathcal{A}^k)}]^{-1}[\widehat{B}^{\mathcal{A}^k}]',$$

where the symbol "$'$" is used to denote dual operators and $R_{L^2(\mathcal{A}^k)}$ is the Riesz map of the space $L^2(\mathcal{A}^k)$, see (16). Hence, the continuous Lagrangian update in Example 1 is

$$\lambda^{\mathcal{A}^k} = [R_{L^2(\mathcal{A}^k)}]^{-1}[\widehat{B}^{\mathcal{A}^k}]' w^k,$$

or

$$R_{L^2(\mathcal{A}^k)}\lambda^{\mathcal{A}^k} = [\widehat{B}^{\mathcal{A}^k}]' w^k.$$

We again refer to [9] for further details about the discretization. Let the superscript notation "$\mathcal{A}^k$" and " : " denote the active indices and all the indices, respectively. The discretized update for the Lagrange multiplier then reads

$$M_v^{\mathcal{A}^k,\mathcal{A}^k}\bar{\lambda}^{\mathcal{A}^k} = M^{\mathcal{A}^k,:}\bar{w}^k.$$

References

[1] M. Benzi, G. H. Golub, and J. Liesen. Numerical solution of saddle point problems. *ACTA NUMERICA*, 14:1–137, 2005.

[2] M. Bergounioux, K. Ito, and K. Kunisch. Primal-dual strategy for constrained optimal control problems. *SIAM Journal on Control and Optimization*, 37(4):1176–1194, 1999.

[3] L. T. Biegler, O. Ghattas, M. Heinkenschloss, and B. van Bloemen Waanders. *Large-Scale PDE-Constrained Optimization*. Springer, 2003.

[4] M. Engel and M. Griebel. A multigrid method for constrained optimal control problems. *Journal of Computational and Applied Mathematics*, 235(15):43684388, 2011.

[5] M. Hinze, R. Pinnau, M. Ulbrich, and S. Ulbrich. *Optimization with PDE Constraints*, volume 23 of *Mathematical Modelling: Theory and Applications*. Springer, 2009.

[6] M. Hinze and M. Vierling. The semi-smooth Newton method for variationally discretized control constrained elliptic optimal control problems; implementation, convergence and globalization. *Optimization Methods and Software*, 27:933–950, 2012.

[7] K. Ito and K. Kunisch. *Lagrange multiplier approach to variational problems and applications*, volume 15 of *Advances in Design and Control*. Society for Industrial and Applied Mathematics (SIAM), Philidelphia, 2008.

[8] K.-A. Mardal and J. B. Haga. Block preconditioning of systems of PDEs. In Anders Logg, Kent-Andre Mardal, and Garth Wells, editors, *Automated Solution of Differential Equations*, pages 635–654. Springer, 2012.

[9] K.-A. Mardal and R. Winther. Preconditioning discretizations of systems of partial differential equations. *Numerical Linear Algebra with Applications*, 18(1):1–40, 2011.

[10] B. F. Nielsen and K.-A. Mardal. Efficient Preconditioners for Optimality Systems Arising in Connection with Inverse Problems. *SIAM Journal on Control and Optimization*, 48(8):5143–5177, October 2010.

[11] B. F. Nielsen and K.-A. Mardal. Analysis of the minimal residual method applied to ill-posed optimality systems. *SIAM Journal on Scientific Computing*, 35(2):785–814, 2013.

[12] C. C. Paige and M. A. Saunders. Solution of sparse indefinite systems of linear equations. *SIAM Journal on Numerical Analysis*, 12(4):617–629, 1975.

[13] A. J. Pullan, M. L. Buist, and L. K. Cheng. *Mathematically Modelling the Electrical Activity of the Heart: From Cell to Body Surface and Back*. World Scientific Publishing Company, 2005.

[14] M. Stoll and A. Wathen. Preconditioning for partial differential equation constrained optimization with control constraints. *Numerical Linear Algebra with Applications*, 19(1):53–71, 2012.

[15] F. Tröltzsch. *Optimal Control of Partial Differential Equations: Theory, Methods and Applications*, volume 112 of *Graduate Studies in Mathematics*. American Mathematical Society: Providence, Rhode Island, 2010.

[16] M. Ulbrich and S. Ulbrich. Primal-dual interior-point methods for PDE-constrained optimization. *Mathematical Programming*, 117(1-2):435–485, 2009.